Geoscience Letters

RESEARCH LETTER

Open Access

Akatsuki LIR observing system simulation experiments evaluated by thermal tides in the Venus atmosphere

Norihiko Sugimoto[1*], Yukiko Fujisawa[1], Nobumasa Komori[1], Hiroki Ando[2], Toru Kouyama[3] and Masahiro Takagi[2]

Abstract

Impacts of temperature assimilation on Venusian thermal tides are investigated by the observing system simulation experiments assuming Akatsuki Longwave Infrared Camera (LIR) observations. Synthetic temperature data are prepared by a Venusian general circulation model (VGCM) to test if LIR temperature data resolves a discrepancy in the structure of thermal tides between observations and the VGCM. They are assimilated at 70 km altitude with several combinations of frequency and horizontal region. The result shows that the three-dimensional structure of thermal tides is significantly improved not only in temperature but also in horizontal wind, even if observations are available only at a limited frequency of 6-hourly or on the dayside. The zonal–mean zonal wind and temperature fields are also modified at 60–80 km altitudes globally through the vertical momentum transport of thermal tides. It would be promising to assimilate Akatsuki LIR observations to produce realistic objective analysis of the Venus atmosphere.

Keywords: Venus atmosphere, Thermal tides, GCM, LETKF data assimilation, Akatsuki

Introduction

The solar heating excites planetary-scale atmospheric waves in a planetary atmosphere, called thermal tides, which generally move with the Sun. The diurnal (semidiurnal) tide is the thermal tide component with a zonal wave number of 1 (2). On Venus, because of the large amount of absorption of the solar flux in the Venusian cloud (Tomasko et al., 1980), the thermal tides are strongly excited in the cloud layer (45–70 km altitudes) (Taylor et al., 1980) and play important roles with respect to the super-rotation through their momentum transport (e.g., Fels and Lindzen, 1974; Horinouchi et al., 2020). The semidiurnal tide has large amplitudes in low latitudes, whereas the diurnal tide is predominant in mid- to high-latitudes above the cloud top level (~ 70 km).

*Correspondence: nori@phys-h.keio.ac.jp

[1] Research and Education Center for Natural Sciences, Department of Physics, Keio University, 4-1-1, Hiyoshi, Kohoku, Yokohama, Kanagawa 223-8521, Japan
Full list of author information is available at the end of the article

In previous studies with Venusian general circulation models (VGCMs), the thermal tides have been investigated in terms of the generation and maintenance mechanisms of super-rotation (Takagi and Matsuda, 2007; Yamamoto and Takahashi, 2009; Lebonnois et al., 2016). Their structure was not fully compared with observations in these studies. We have developed a VGCM named AFES-Venus (an atmospheric GCM for the Earth Simulator (AFES) for Venus) (Sugimoto et al., 2014a) on the basis of AFES (Ohfuchi et al., 2004). In AFES-Venus, a weakly stratified layer observed in the cloud layer (Tellmann et al., 2009) is taken into account, which enables us to reproduce the realistic super-rotation, planetary-scale waves (Sugimoto et al., 2014b), a polar vortex with cold collar (Ando et al., 2016), and planetary-scale streak features (Kashimura et al., 2019). A detailed structure of the thermal tides was also investigated (Takagi et al., 2018). However, recent observations show that the zonal phase distribution of thermal tides reproduced in AFES-Venus was not consistent

with radio occultation (RO) measurements of Venus Express and Akatsuki (Ando et al., 2018) and Longwave Infrared Camera (LIR) observations of Akatsuki (Kouyama et al., 2019). Compared to these observations, the temperature distribution reproduced in AFES-Venus was shifted by about 30° in the longitudinal direction near the cloud top (Ando et al., 2018). The RO measurements also indicate that the static stability reproduced in AFES-Venus is not consistent with that in the real Venus atmosphere (Ando et al., 2020). To resolve these inconsistencies, Takagi et al. (2022) improved the solar heating and radiative cooling process that depend on distributions of the cloud and unknown UV absorber (Haus et al., 2015). As a result, the structure of thermal tides is largely improved (Suzuki et al., 2022), though the phase discrepancy is not completely resolved. Since there is a large uncertainly in the distributions of cloud and unknown UV absorber, it is quite difficult to correctly reproduce the thermal tides by improving the VGCM. Therefore, data assimilation would be useful to reproduce thermal tides to be three dimensionally consistent with the observations.

Data assimilation has been widely used in the Earth atmosphere to advance numerical weather forecasting and provide objective analysis by reducing errors between models and observations. The data assimilation also allows us to perform observing system simulation experiments (OSSEs) to evaluate hypothetical observations before they become a reality. Recently, a data assimilation system for Venus (ALEDAS-V) has been developed based on AFES local ensemble transform Kalman filter (LETKF) (Sugimoto et al., 2017). Using ALEDAS-V and horizontal winds at the dayside cloud top derived from ultraviolet (UV) Venus images taken by Venus Monitoring Camera (VMC) onboard Venus Express, Sugimoto et al. (2019b) demonstrated that the horizontal wind assimilation effectively improves the structures of thermal tides and general circulation. However, temperature observations, which are abundantly provided by LIR observations of Akatsuki and could be used for the data assimilation, have not been assimilated into VGCM so far. Before we assimilate the LIR temperature observations, it is necessary to perform OSSEs to evaluate its effectiveness and/or conditions for it to work effectively. In the present study, we investigate the impact of the temperature assimilation on the thermal tides and the general circulation using synthetic temperature observations produced by AFES-Venus assuming Akatsuki LIR observations.

Experimental setup

Venus general circulation model (AFES-Venus)

AFES-Venus solves the primitive equations on a sphere with simplified physical processes without topography (Sugimoto et al., 2014a). The resolution is a 128 by 64 horizontal grid with 60 vertical layers (T42L60, where T and L denote the triangular truncation number for spherical harmonics and vertical levels, respectively). Then, the horizontal and vertical grid intervals are ~ 300 km and ~ 2 km, respectively, with constant thickness from the ground to 120 km altitude. The horizontal second-order hyper eddy viscosity is applied with a damping time of 0.1 Earth days for the maximum wave number component. The vertical eddy diffusion is also used with a constant coefficient of 0.15 $m^2 s^{-1}$. The surface friction is represented by Rayleigh friction with a damping time of 0.5 Earth days. A sponge layer is also introduced only to the eddy components above 80 km with damping times gradually decreasing with height. Convective adjustment is applied when the static stability becomes negative. The solar heating is based on Tomasko et al. (1980) and infrared radiative transfer is simplified by a Newtonian cooling scheme (c.f., Crisp, 1989). The horizontally uniform temperature field based on Venus International Reference Atmosphere (VIRA) (Seiff et al., 1985) is used for the reference temperature distribution of the Newtonian cooling. Details are described in the previous papers (Sugimoto et al., 2014a, b).

As an initial state of the velocity field, we prepare an idealized super rotating flow; the zonal wind increases linearly with height from the ground to 70 km and reaches 100 m s^{-1} at the equator. In the meridional direction, the idealized super rotating flow is in solid-body rotation. The initial temperature distribution is in gradient wind balance with the zonal wind field. Note that Venus rotates very slowly, but the Coriolis force appears in a frame of reference rotating with its fast super-rotation. From this initial state, nonlinear numerical simulations are performed for more than four Earth years. We use quasi-equilibrium data sets sampled at an 8-h interval to produce initial conditions for each 31-member ensemble for LETKF. We have confirmed that while the zonal mean fields are almost similar between ensemble members, the eddy fields are totally different. Note that a fully developed super-rotation could be obtained from a motionless state with a small vertical viscosity by a very long time-integration (~ 3000 Earth years) (Sugimoto et al., 2019a). To save computational time, the idealized super rotating flow is used in the present study. Note also that the direction of the planetary rotation is the same as that of Earth (eastwards is positive). This is the conventional direction of rotation used in the fields of meteorology and geophysical fluid dynamics and it is convenient

for those familiar with the Earth's atmospheric dynamics. The dynamics are consistent to those in the real atmosphere of Venus regardless of the direction of planetary rotation. Reversing the direction of longitude and the sign of zonal wind in the present simulation gives a flow field consistent with observations.

Data assimilation system for Venus (ALEDAS-V)

The LETKF has been widely used in the terrestrial meteorology (Miyoshi et al., 2007; Yamazaki et al., 2017) and has also been applied to the Martian atmosphere (Greybush et al., 2012). The best estimate with minimum error variance in models and observations can be obtained by an approximation of the Kalman filter. A square root filter (Whitaker and Hamill, 2002) of the ensemble Kalman filter (Evensen, 1994) is used in the LETKF. Only observations within a prescribed horizontal and vertical distance are considered (localization; Ott et al., 2004). The LETKF uses the technique of ensemble transform Kalman filter (Bishop et al., 2001) for computational efficiency.

ALEDAS-V uses 31-member ensemble and 10% multiplicative spread inflation (Sugimoto et al., 2017; 2019b). We also use the localization parameters of 400 km in horizontal and $\log P = 0.4$ in vertical, where P is pressure. We assume random Gaussian errors with a 3.0 K standard deviation for the temperature field based on LIR's uncertainty in absolute temperature (Fukuhara et al., 2011). The observations are assigned to hourly time slots (Hunt et al., 2004) and the data assimilation cycle is 6 h, namely, 7-h time slots are assigned at each analysis in four-dimensional LETKF. Therefore, we use observations from 3 h before to 3 h after to the target assimilation time every 6 h. Note that the dependency of the results on localization parameters, observation errors, and ensemble members has been checked in the previous studies (Sugimoto et al. 2017; 2019b).

The synthetic temperature observations are produced from temperature fields at 70 km obtained in AFES-Venus to mimic Akatsuki LIR observations and assimilated them at the same altitude. To take into account of the phase discrepancy of thermal tides between observations and AFES-Venus, we produced the synthetic temperature observations by zonally shifting the temperature field obtained in AFES-Venus by 30°. The horizontal resolution of the synthetic temperature observations is the same as that of AFES-Venus. Many of LIR observations are conducted around the apoapsis of Akatsuki orbit (~360,000 km), where the spatial resolution of LIR (0.05 degree/pixel (Fukuhara et al., 2011)) corresponds to ~300 km (~3° both in the longitudinal and latitudinal directions). When Akatsuki is close to periapsis the LIR only observes a fraction of the Venus disk. However, since Akatsuki is in a 10-day highly elliptical orbit, it passes around periapsis in a very short time (~8.5 h). After ~24 h, the LIR covers a wide area again that is almost the same as the observation from apoapsis. Then, the LIR continuously observes almost hemisphere of Venus at 1- or 2-h intervals around apoapsis. While they can observe both the dayside and nightside of Venus, limited local time observations are accumulated due to the slow transition of the local time. Typically, it takes ~4 months to make a transition between dayside and nightside. Since LIR observes thermal radiations emitted from 45 to 85 km altitudes (Taguchi et al., 2007), which strongly depend on the cloud structure, there is uncertainty of the altitude of observation. We use temperature fields at a fixed altitude of 70 km (the cloud top level) for the synthetic observations for simplicity but a sensitivity study at 65 km altitude has also been performed (see Additional file 1: S4). We prepare several cases of the synthetic observations with different frequencies from hourly (h1) to daily (h24) and global, dayside (ds), and nightside (ns) regions for OSSEs for a sensitivity check (Table 1; see also Additional file 1: Fig. S1). The data assimilation is performed for one Earth month from 1st January, 5th year. We will compare the results of OSSEs with free run forecast (frf) of AFES-Venus (without data assimilation). Note that the synthetic temperature observations are the same as those of free run forecast except for the zonal shift by 30°.

Headings in the vertical column indicate regions of observations (global, dayside, and nightside) and headings in the horizontal row indicate frequencies of observations (hourly to daily).

Results

Time evolution

Figure 1 shows longitude–time cross sections of temperature deviations at 70 km altitude and the equator. The black lines indicate the sub-solar point. The

Table 1 Cases of synthetic temperature observations for observing system simulation experiments

Frequency/Area	Hourly	2-hourly	4-hourly	6-hourly	12-hourly	24-hourly (daily)
Global	h1	h2	h4	h6	h12	h24
Dayside	h1_ds	h2_ds	h4_ds	h6_ds	h12_ds	h24_ds
Nightside	h1_ns	h2_ns	h4_ns	h6_ns	h12_ns	h24_ns

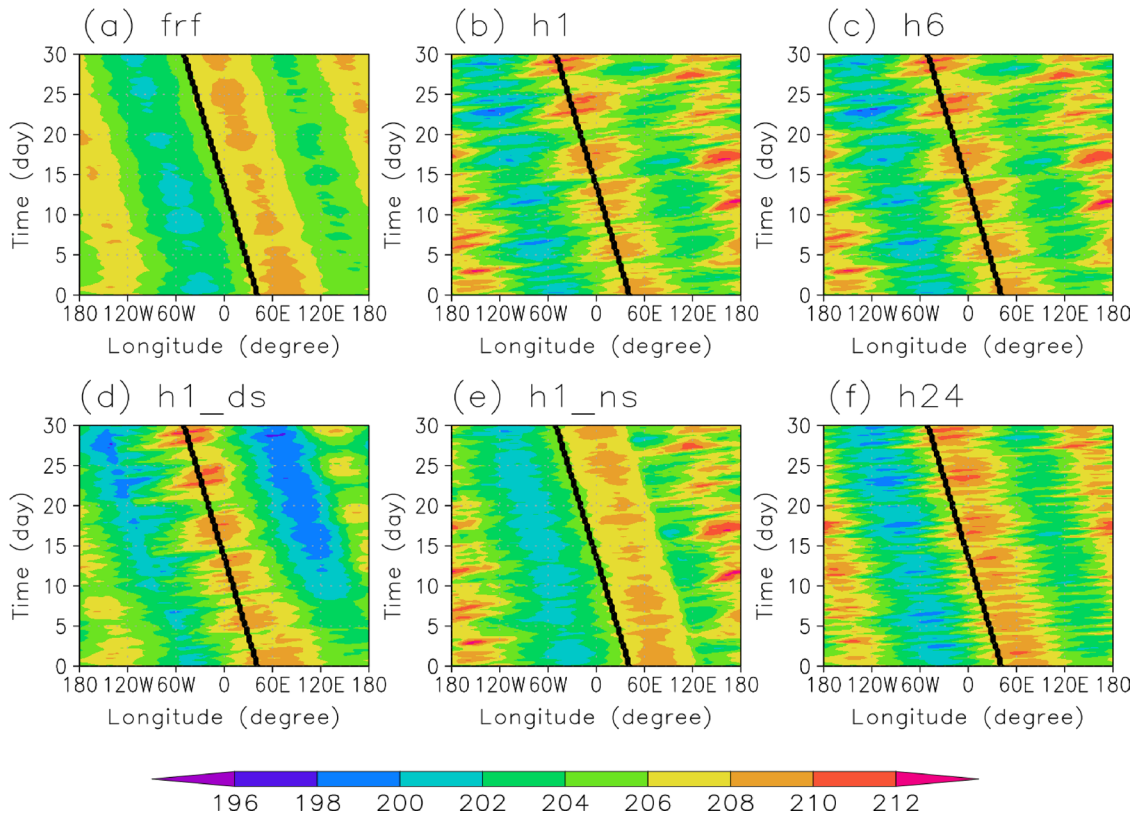

Fig. 1 Longitude–time cross sections of temperature (K) deviations at 70 km altitude and the equator. **a** Free run forecast (frf) of AFES-Venus (without data assimilation), hourly observations on **b** global (h1), **d** dayside (h1_ds), **e** nightside (h1_ns), and **c** 6-hourly (h6) and **f** 24-hourly (h24) observations on global are shown, respectively. The black lines indicate the sub-solar point

semidiurnal tide is predominant near the equator in the temperature field as shown in previous studies (Takagi et al., 2018; Ando et al., 2018; Suzuki et al., 2022). The thermal tides gradually move to westward with the sub-solar point, because the directions of the planetary rotation are assumed to be eastward (positive) in the present study. The sign of temperature changes at the sub-solar point for the case of frf (Fig. 1a), while the temperature at the sub-solar point is positive for the cases of h1, h6, and h1_ds, in which observations are assimilated every 1-h and 6-h globally and every 1-h on the dayside (Fig. 1b–d). These results show that the phase discrepancy is resolved and the temperature field is improved in these cases. On the other hand, for the case of h1_ns, in which observations are assimilated hourly on the nightside, the temperature on the dayside is not modified by the data assimilation (Fig. 1e). In the case of h24, the improvement is not so large, because the observations are available only once a day (Fig. 1f). See also animation (Additional file 2) for the cases of h1, h2, h4, h6, h12, and h24 for comparison. The improvements are similar between the cases of h1 to h6. The results of the case of h12 are better than those of h24, but are not as good as those of h1 to h6.

Horizontal structure

To extract the structure of thermal tides, we calculate the composite mean of the horizontal distributions of temperature and horizontal wind over 30 Earth days at the sub-solar point. The results are shown in Fig. 2. The sub-solar point (12:00 LT) is located at 0°E longitude (fixed at the center of each panel). It is clearly observed in the temperature field that the semidiurnal component (a tidal component of wave number 2) of thermal tides is predominant in low-latitudes, while the diurnal component is predominant in mid- and high-latitudes. In the temperature field for the case of frf (Fig. 2a), the sign of temperature deviation changes around noon, and a local maximum appears at ~ 30°E–45°E longitudes (14–15 LT) around the equator. This distribution indicates that the horizontal structures of the semidiurnal tide reproduced in AFES-Venus are not consistent with the RO (Fig. 2a in Ando et al., 2018) and LIR (Fig. 2a in Kouyama et al., 2019) observations of

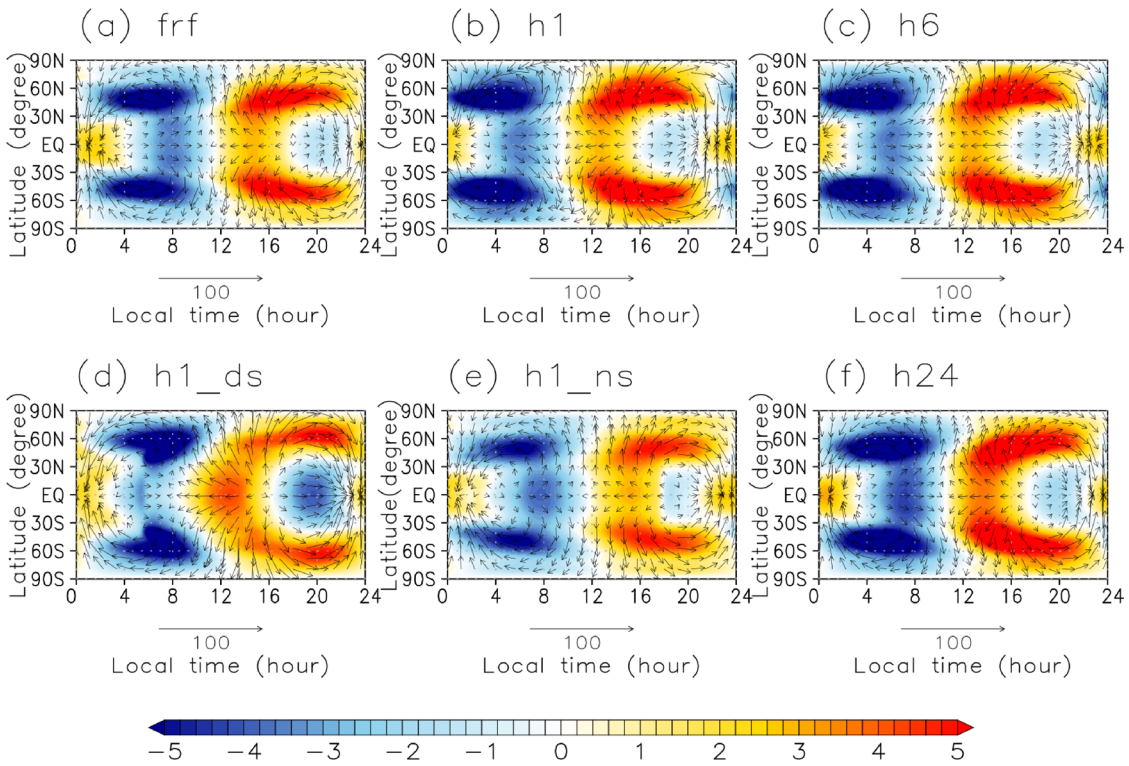

Fig. 2 Horizontal distributions of horizontal wind (vector, m s^{-1}) and temperature deviations (color, K) associated with the thermal tides at the cloud top level (~70 km). The cases of **a** frf, **b** h1, **c** h6, **d** h1_ds, **e** h1_ns, and **f** h24 are shown. These distributions are calculated by the composite means over 30 Earth days at the sub-solar point (fixed at the center of each panel)

Akatsuki as mentioned in "Introduction" section. The distribution of the horizontal wind in low-latitudes is also not consistent with that derived from Venus Express data (Fig. 1 in Sugimoto et al., 2019b) at the cloud top level. Namely, the distribution of semidiurnal tide reproduced in AFES-Venus was shifted by about 30° in the longitudinal direction near the cloud top in both temperature and horizontal wind fields.

As shown in Fig. 2b–d, the phase distributions of the thermal tides in low-latitudes are improved by assimilating the temperature by ALEDAS-V in both the horizontal wind and temperature fields for the cases of h1, h6, and h1_ds, in which both the local minimum of zonal wind and the local maximum of temperature appear around noon around the equator at the cloud top level (~70 km). Note that for cases h1_ns and h24, improvements of the phase distributions of the thermal tides seem to be insufficient, because the observations are available only on the nightside or once an Earth day (Fig. 2e, f). It should be noted that the horizontal winds for the case of h1_ds change quite significantly, but they are not consistent with those derived from Venus Express data (Fig. 1 in Sugimoto et al., 2019b) at the cloud top level.

Vertical structure

To investigate how the impact of data assimilation at 70 km altitude extends in the vertical direction, the temperature deviations associated with the thermal tides (calculated by the composite means over 30 Earth days at the sub-solar point) in a longitude–height section on the equator are shown in Fig. 3. Again, the sub-solar point (12:00 LT) is located at 0°E longitude (fixed at the center of each panel). Amplitudes are scaled with the square root of the density at each altitude divided by the fixed density at 70 km altitude for visibility. The phase distributions are changed at 65–75 km levels for the temperature deviations. It is clearly shown that the phases of the semidiurnal tide are significantly modified in these levels for the cases of h1, h6, and h1_ds. While the temperature field has an upright structure for the case of frf, those obtained for the cases of h1, h6, and h1_ds are tilted. These titled features are more consistent with the RO observations of Akatsuki (Fig. 2a in Ando et al., 2018).

Zonal wind

Since the thermal tides propagate vertically, it is expected that they could give large impacts on general circulation of the Venus atmosphere. Figure 4 shows the zonal–mean

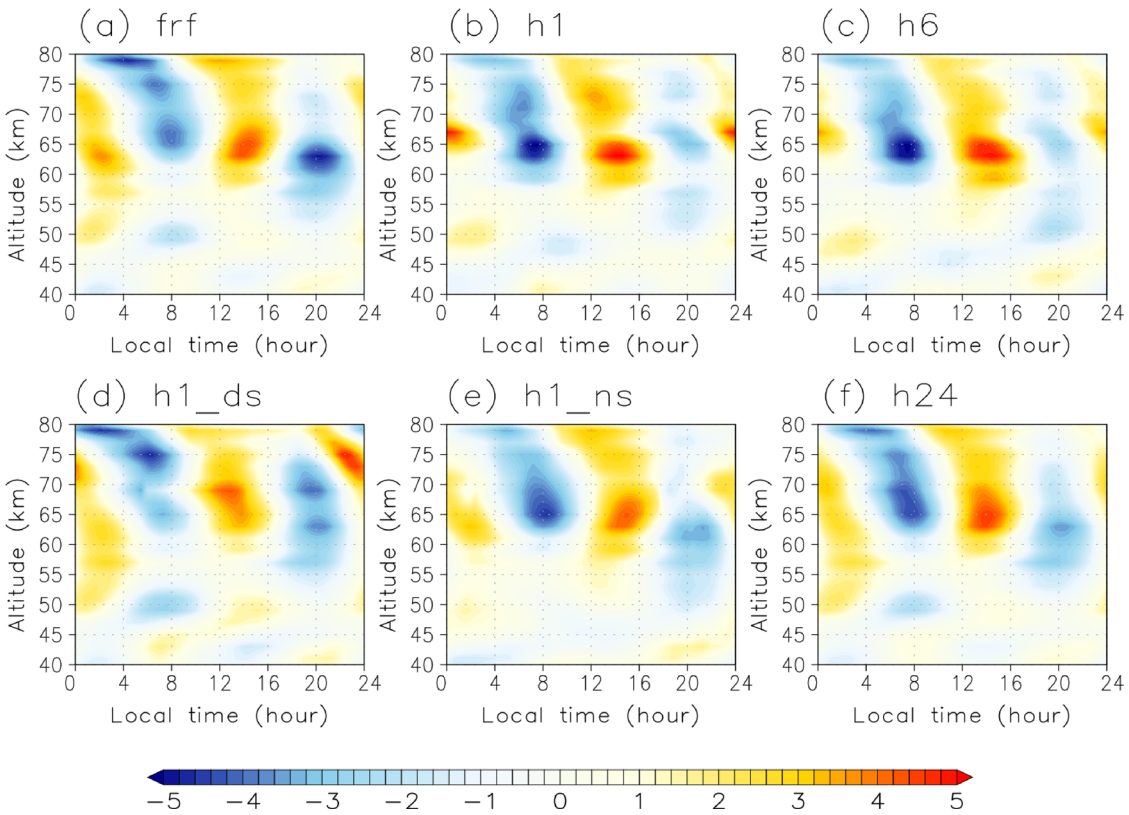

Fig. 3 Vertical distributions of temperature (K) deviations associated with the thermal tides at the equator. The cases of **a** frf, **b** h1, **c** h6, **d** h1_ds, **e** h1_ns, and **f** h24 are shown. These distributions are calculated by the composite means over 30 Earth days at the sub-solar point (fixed at the center of each panel). Amplitudes are multiplied by a factor of $100\sqrt{\sigma}$ for visibility, where σ is a scaled pressure level in the sigma coordinate system

zonal wind (color) and temperature fields (white contours) obtained at the final day in a latitude–height cross section. The zonal–mean zonal wind and temperature fields are significantly modified (Fig. 4b–e) as a result of the data assimilation except for the case of h24 (Fig. 4f). The zonal–mean zonal wind above the cloud top region (~65–80 km) substantially decreases by about 20 m s^{-1} for the cases of h1, h6, and h1_ds (Fig. 4b–d), while it increases about 10 m s^{-1} for the cases of h1_ns (Fig. 4e). We have also calculated root mean square distances (RMSDs) in zonal wind from the free run forecast at 70 km altitude for each case (Additional file 1: Figs. S2–S4). The temperature field is also modified especially in high-latitudes around the cloud top level (~70 km). It might be surprising that the zonal–mean zonal wind changes significantly in the present results, because the zonal–mean component of the synthetic temperature field is balanced with the zonal–mean zonal wind, thus the temperature assimilation could not change the zonal–mean zonal wind directly. However, the temperature assimilation could modify horizontal wind locally, because horizontal wind disturbances are related to their temperature deviations through the thermal wind balance. Then, the improvement of the three-dimensional structure of thermal tides would have large impacts on the general circulation through the momentum and heat transports associated with the thermal tides.

Vertical momentum flux

It is interesting that the zonal–mean zonal flow changes in different ways for the dayside and nightside temperature assimilations (Fig. 4d, e). To investigate the reason for the modification of the zonal–mean field shown in Fig. 4, the vertical momentum flux associated with the thermal tides (color) in a latitude–height cross section averaged over the last 30 Earth days are analysed, as shown in Fig. 5. For the case of frf, the thermal tides decelerate the super-rotation in low-latitudes, while they accelerate it in mid-latitudes at 60–75 km altitudes (Fig. 5a). In contrast, for the cases of h1 and h1_ds, the super-rotation is decelerated more strongly in low-latitudes (Fig. 5b, c). The acceleration of super-rotation in mid-latitudes almost vanishes in the case of h1_ds (Fig. 5c). As a result, the super-rotation is decelerated substantially in these cases (Fig. 4b–d). For the case of h1_ns, the vertical momentum flux is similar to those obtained for the case of frf,

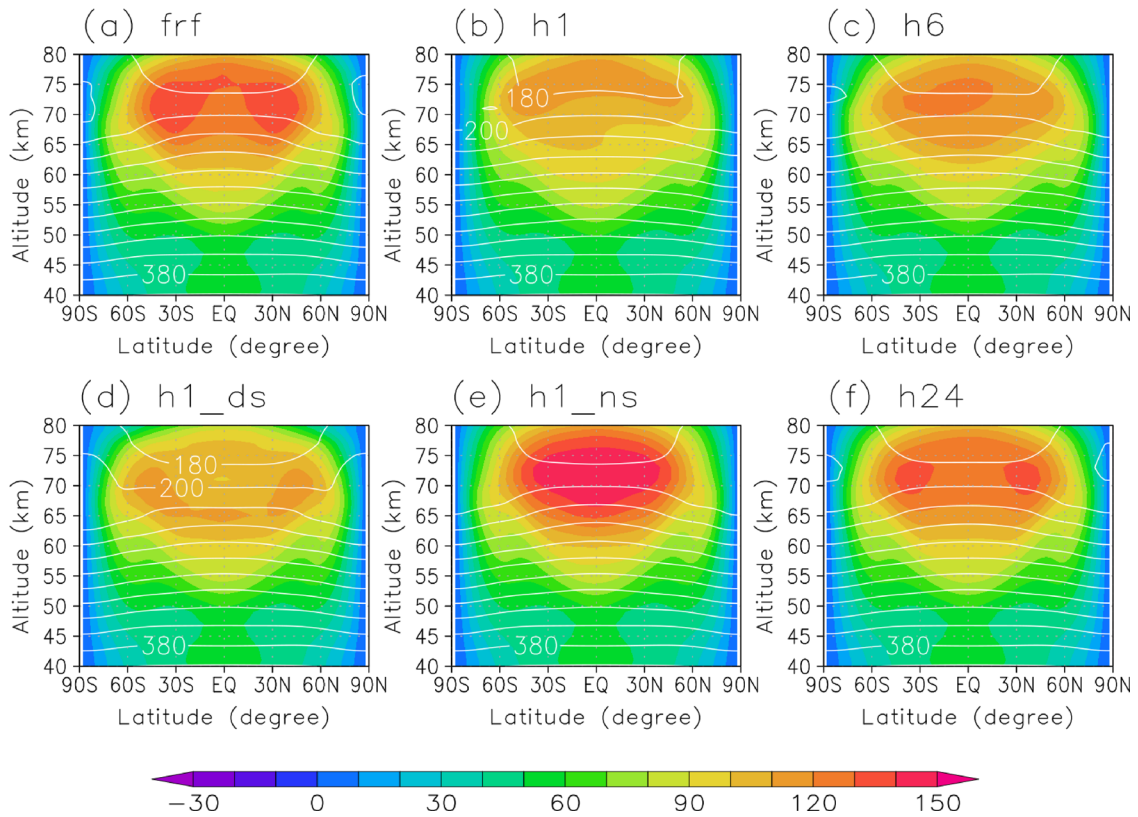

Fig. 4 Zonal–mean zonal wind (colors, m s^{-1}) and temperature (white contours, K) in a latitude–height cross section at the final day. The cases of **a** frf, **b** h1, **c** h6, **d** h1_ds, **e** h1_ns, and **f** h24 are shown

but the deceleration at 75–80 km altitudes in the low-latitudes is weaker than that of frf. Then, the super-rotation is accelerated around 75 km altitudes (Fig. 4e).

Summary and discussion

In the present study, we investigated impacts of the data assimilation of temperature on the thermal tides and the general circulation in the Venus atmosphere by observing system simulation experiments using the data assimilation system, ALEDAS-V (Sugimoto et al., 2017). The synthetic temperature observations are produced by the VGCM (AFES-Venus) to simulate observations of infrared images taken by Longwave Infrared Camera (LIR) onboard the Akatsuki Venus Climate Orbiter. The thermal tides obtained in an original run of AFES-Venus are inconsistent with observations; their phase distributions at the cloud top level are out of phase by about 30° in the zonal direction from those obtained by the recent observations (Ando et al., 2018; Kouyama et al., 2019). This inconsistency was successfully resolved by the data assimilation of the temperature fields, even if the temperature observations were available only at the cloud top on the dayside or every 6 h (i.e., the cases of h1, h2, h4, h6, and h1_ds resulted in successful assimilations, while those of h1_ns, h12, and h24 did not). Furthermore, the global structures of zonal–mean zonal wind and temperature were also improved significantly. These results suggest that the improvement of the thermal tides would have large impacts on the general circulation through changes of their momentum and heat transports.

In the previous work (Sugimoto et al., 2019b), the zonal–mean zonal wind was significantly decelerated by the assimilation of horizontal wind at the cloud top. The result is understandable, because the zonal wind derived from Venus Monitoring Camera (VMC) is much slower than that in AFES-Venus. Compared with their result, the present one is surprising, because the temperature assimilation at the cloud top also improves the horizontal wind field at 60–80 km altitudes significantly. Since the horizontal wind is related to the temperature through the thermal wind balance, the temperature assimilation could have impacts on the wind field. However, the zonal–mean component of the synthetic temperature field is unchanged and balanced with the zonal–mean zonal wind, so that the temperature assimilation could not change the zonal–mean zonal wind directly in the

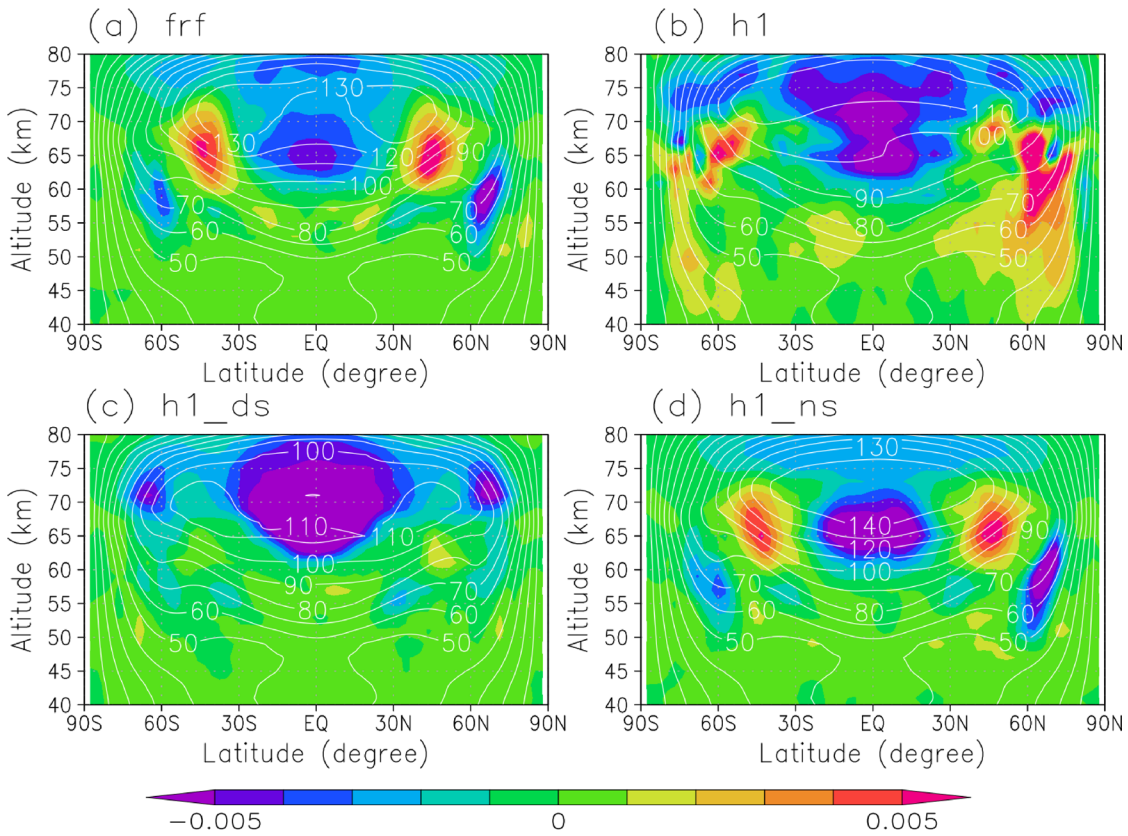

Fig. 5 Zonal–mean zonal wind (contours, m s^{-1}) and vertical momentum flux (colours, 10^{-3} kg m^{-1} s^{-2}) in a latitude–height cross section averaged over the last 30 Earth days. The cases of **a** frf, **b** h1, **c** h1_ds, and **d** h1_ns are shown

present study. Nevertheless, the assimilation on the dayside temperature decelerates (and improves) the superrotation. The temperature structure of the thermal tides has a large impact on the zonal–mean zonal wind through its momentum transport. We have also confirmed that while the phases of thermal tide go back to the original ones at about ~ 10 days, RMSDs show that a difference of more than 10 m/s remains between the assimilation forecast and the free run forecast even after one month for all the tested cases except h24 (see Additional file 1: S5). The present results suggest that the assimilation of Akatsuki LIR observations is quite promising to reproduce realistic structures of the Venus atmosphere. Note that the assimilation of the nightside temperature does not improve the thermal tides and the zonal–mean zonal wind. Because the Akatsuki LIR observations are available in both dayside and nightside, we have to check their assimilation impact carefully in future work.

For future, we will carry out the Akatsuki LIR temperature assimilation to produce objective analysis as well as Akatsuki UV horizontal wind. However, to assimilate the LIR temperature data effectively, there are some difficulties to determine the sensing altitude and treat the vertical integrated temperature observations (Taguchi et al., 2007). We conducted a sensitivity study assimilating temperatures at an altitude of 65 km instead of 70 km (see Additional file 1: S4) and confirmed that the results are almost unchanged at 65 km, namely, the phases of thermal tide are improved sufficiently (Additional file 1: Figs. S5 and S6). However, the phases of thermal tide at 70 km are not improved enough (Additional file 1: Fig. S7). Therefore, we have to check carefully how the assimilation result depends on the sensing altitude and vertical localizations of the LIR temperature observations. Alternatively, an infrared radiative transfer model could be introduced to directly assimilate LIR radiances in the future.

Supplementary Information

The online version contains supplementary material available at https://doi.org/10.1186/s40562-022-00253-8.

Additional file 1. Explanation of Supplementary Information and additional figures.

Additional file 2. Animation file.

Additional file 3. Data set.

Acknowledgements
This study was conducted under the joint research project of the Earth Simulator with title "High resolution general circulation simulation of Venus and Mars atmosphere using AFES". The work is partly supported by JSPS KAKENHI grants Numbers JP19H0197, JP19H05605, JP19K14789, JP20H01958, and JP20K04064. The authors thank two anonymous reviewers for useful comments. The GFD-DENNOU Library was used for creating figures. Results from the GCM simulations performed in this paper are provided as supplementary information.

Author contributions
NS developed the AFES-Venus and ALEDAS-V with a help of NK and MT. YF performed numerical experiments with a help of NS. NS and YF analyzed obtained data with a help of HK. NS wrote the first draft and final manuscript. All the authors including HA, TK and MT contributed to the scientific discussion. All authors read and approved the final manuscript.

Funding
The work is partly supported by JSPS KAKENHI grants Numbers JP19H0197, JP19H05605, JP19K14789, JP20H01958, and JP20K04064.

Availability of data and materials
Results from the GCM simulations performed in this paper are provided as supplementary information (Additional file 3).

Declarations

Competing interests
The authors declare that they have no competing interests.

Author details
[1]Research and Education Center for Natural Sciences, Department of Physics, Keio University, 4-1-1, Hiyoshi, Kohoku, Yokohama, Kanagawa 223-8521, Japan. [2]Faculty of Science, Kyoto Sangyo University, Kyoto 603-8555, Japan. [3]Digital Architecture Research Center, National Institute of Advanced Industrial Science and Technology, Tokyo 135-0064, Japan.

Received: 9 July 2022 Accepted: 2 November 2022
Published online: 16 November 2022

References

Ando H, Sugimoto N, Takagi M, Kashimura H, Imamura T, Matsuda Y (2016) The puzzling Venusian polar atmospheric structure reproduced by a general circulation model. Nat Commun 7:10398. https://doi.org/10.1038/ncomms10398

Ando H, Takagi M, Fukuhara T, Imamura T, Sugimoto N, Sagawa H et al (2018) Local time dependence of the thermal structure in the Venusian equatorial upper atmosphere: comparison of Akatsuki radio occultation measurements and GCM results. J Geophys Res Planets. https://doi.org/10.1029/2018JE005640

Ando H et al (2020) Thermal structure of Venus atmosphere from sub-cloud region to the mesosphere observed by radio occultation. Sci Rep 10:3448. https://doi.org/10.1038/s41598-020-59278-8

Bishop CH, Etherton BJ, Majumdar SJ (2001) Adaptive sampling with the ensemble transform Kalman filter. Part I: theoretical aspects. Mon Wea Rev 129:420–436. https://doi.org/10.1175/1520-0493(2001)129<0420:ASWTET>2.0.CO;2

Crisp D (1989) Radiative forcing of the Venus mesosphere. II. Thermal fluxes, cooling rates, and radiative equilibrium temperatures. Icarus 77:391–413

Evensen G (1994) Sequential data assimilation with a nonlinear quasi-geostrophic model using Monte Carlo methods to forecast error statistics. J Geophys Res 99(C5):10143–10162. https://doi.org/10.1029/94JC00572

Fels SB, Lindzen RS (1974) The interaction of thermally excited gravity waves with mean flows. Geophys Fluid Dyn 6:149–191. https://doi.org/10.1080/03091927409365793

Fukuhara et al (2011) LIR: Longwave Infrared Camera onboard the Venus orbiter Akatsuki. Earth Planet Space 63:1009–1018

Greybush SJ et al (2012) Ensemble Kalman filter data assimilation of Thermal Emission Spectrometer temperature retrievals into a Mars GCM. J Geophys Res 117:E11008. https://doi.org/10.1029/2012JE004097

Haus R, Kappel D, Arnold G (2015) Radiative heating and cooling in the middle and lower atmosphere of Venus and responses to atmospheric and spectroscopic parameter variations. Planet Space Sci 117:262–294

Horinouchi T et al (2020) How waves and turbulence maintain the super-rotation of Venus' atmosphere. Science 368:405–409

Hunt BR et al (2004) Four-dimensional ensemble Kalman filtering. Tellus 56A:273–277. https://doi.org/10.3402/tellusa.v56i4.14424

Kashimura H, Sugimoto N, Takagi M, Ohfuchi W, Enomoto T, Nakajima K et al (2019) Planetary-scale streak structure reproduced in a Venus atmospheric simulation. Nat Commun 10:23. https://doi.org/10.1038/s41467-018-07919-y

Kouyama T, Taguchi M, Fukuhara T, Imamura T, Horinouchi T, Sato TM et al (2019) Global structure of thermal tides in the upper cloud layer of Venus revealed by LIR on board Akatsuki. Geophys Res Lett 46:9457–9465. https://doi.org/10.1029/2019GL083820

Lebonnois S, Sugimoto N, Gilli G (2016) Wave analysis in the atmosphere of Venus below 100 km altitude, simulated by LMD Venus GCM. Icarus 278:38–51

Miyoshi T, Yamane S, Enomoto T (2007) The AFES-LETKF experimental ensemble reanalysis: ALERA. SOLA 3:45–48. https://doi.org/10.2151/sola.2007-012

Ohfuchi W, Nakamura H, Yoshioka MK, Enomoto T, Takaya K, Peng X, Yamane S, Nishimura T, Kurihara Y, Ninomiya K (2004) 10-km mesh meso-scale resolving simulations of the global atmosphere on the Earth Simulator, -Preliminary outcomes of AFES (AGCM for the Earth Simulator)-. J Earth Simulator 1:8–34. https://doi.org/10.32131/jes.1.8

Ott E et al (2004) A local ensemble Kalman filter for atmospheric data assimilation. Tellus 56A:415–428

Seiff A, Schofield JT, Kliore AJ, Taylor FW, Limaye SS, Revercomb HE et al (1985) Models of the structure of the atmosphere of Venus from the surface to 100 kilometers altitude. Adv Space Res 5:3–58

Sugimoto N, Takagi M, Matsuda Y (2014a) Baroclinic instability in the Venus atmosphere simulated by GCM. J Geophys Res Planets 119:1950–1968. https://doi.org/10.1002/2014JE004624

Sugimoto N, Takagi M, Matsuda Y (2014b) Waves in a Venus general circulation model. Geophys Res Lett 41:7461–7467. https://doi.org/10.1002/2014GL061807

Sugimoto N, Yamazaki A, Kouyama T, Kashimura H, Enomoto T, Takagi M (2017) Development of an ensemble Kalman filter data assimilation system for the Venusian atmosphere. Sci Rep 7:9321. https://doi.org/10.1038/s41598-017-09461-1

Sugimoto N, Takagi M, Matsuda Y (2019a) Fully developed super-rotation driven by the mean meridional circulation in a Venus GCM. Geophys Res Lett 46:1776–1784. https://doi.org/10.1029/2018GL080917

Sugimoto N, Kouyama T, Takagi M (2019b) Impact of data assimilation on thermal tides in the case of Venus Express wind observation. Geophys Res Lett 46:4573–4580. https://doi.org/10.1029/2019GL082700

Suzuki A, Takagi M, Ando H, Imai M, Sugimoto N, Matsuda Y (2022) A sensitivity study of the thermal tides in the Venusian atmosphere: structures and dynamical effects on the superrotation. J Geophys Res Planets. 127:e2022JE007243. https://doi.org/10.1029/2022JE007243

Taguchi M, Fukuhara T, Imamura T, Nakamura M, Iwagami N, Ueno M et al (2007) Longwave infrared camera onboard the venus climate orbiter. Adv Space Res 40(6):861–868. https://doi.org/10.1016/j.asr.2007.05.085

Takagi M, Matsuda Y (2007) Effects of thermal tides on the Venus atmospheric superrotation. J Geophys Res 112:D09112. https://doi.org/10.1029/2006JD007901

Takagi M, Sugimoto N, Ando H, Matsuda Y (2018) Three dimensional structures of thermal tides simulated by a Venus GCM. J Geophys Res Planets 123:335–352. https://doi.org/10.1002/2017JE005449

Takagi M, Ando H, Sugimoto N, Matsuda Y (2022) A GCM study on the 4-day and 5-day waves in the Venus atmosphere. J Geophys Res Planets. 127:e2021JE007164. https://doi.org/10.1029/2021JE007164

Taylor FW, Beer R, Chahine MT, Diner DJ, Elson LS, Haskins RD, McCleese DJ, Martonchik JV, Reichley PE (1980) Structure and meteorology of the middle atmosphere of Venus: infrared remote sensing from the Pioneer Orbiter. J Geophys Res 85:7963–8006

Tellmann S, Patzold M, Hausler B, Bird MK, Tyler GL (2009) Structure of the Venus neutral atmosphere as observed by the Radio Science experiment VeRa on Venus Express. J Geophys Res 114:E00B36

Tomasko MG, Doose LR, Smith PH, Odell AP (1980) Measurement of the flux of sunlight in the atmosphere of Venus. J Geophys Res 85:8167–8186

Whitaker JS, Hamill TM (2002) Ensemble data assimilation without perturbed observations. Mon Wea Rev 130:1913–1924. https://doi.org/10.1175/1520-0493(2002)130<1913:EDAWPO>2.0.CO;2

Yamamoto M, Takahashi M (2009) Dynamical effects of solar heating below the cloud layer in a Venus-like atmosphere. J Geophys Res 114:E12004. https://doi.org/10.1029/2009JE003381

Yamazaki A, Enomoto T, Miyoshi T, Kuwano-Yoshida A, Komori N (2017) Using observations near the poles in the AFES-LETKF data assimilation system. SOLA 13:41–46. https://doi.org/10.2151/sola.2017-008

Publisher's Note